Solar Energy Materials & Solar Cells 222 (2021) 110908

Contents lists available at ScienceDirect

Solar Energy Materials and Solar Cells

journal homepage: http://www.elsevier.com/locate/solmat

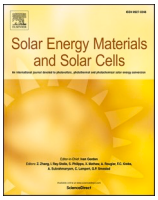

Effect of dew and rain on photovoltaic solar cell performances

Eylul Simsek [a], Megan J. Williams [a], Laurent Pilon [a,b,c,*]

[a] Mechanical and Aerospace Engineering Department, University of California, Los Angeles, Los Angeles, CA, 90095-1597, USA
[b] California NanoSystems Institute, University of California, Los Angeles, Los Angeles, CA, 90095, USA
[c] Institute of the Environment and Sustainability, University of California, Los Angeles, CA, 90095, USA

ARTICLE INFO

Keywords:
Dropwise condensation
Photovoltaic solar cell
Reflectance
Dew
Rain
Efficiency

ABSTRACT

This study investigates experimentally the impact of droplets on the performance of solar photovoltaic (PV) cells due to dropwise condensation or rain falling on their cover. Dew formation occurs frequently in various climates including in semi-arid regions suitable to PV cell deployment. Then, droplets present on the cover of solar cells can negatively affect the cell power generation and efficiency due to optical effects. Here, semi-transparent glass covers were prepared without or with surface treatments and covered with acrylic droplets with contact angle ranging between 25° and 77° and surface area coverage between 19% and 49%. The current vs. voltage curves of commercial polycrystalline silicon solar cells with dry and droplet-covered glass covers were measured under simulated solar irradiation at incidence angle varying between 0° and 85°. For incident angles $\theta_i \leq 30°$, the droplets did not affect the performance of the PV cells. However, for incident angles $\theta_i > 30°$, the presence of droplets caused the maximum power and energy conversion efficiency of the PV cells to decrease significantly, particularly for large droplet contact angle and/or surface area coverage. Such performance degradation was attributed to the fact that the incident light was back-scattered through the droplets instead of being trapped by total internal reflection at the cover/air interface before being eventually absorbed by the solar cell. The study also shows that the hourly energy production of PV cells can decrease significantly with dew formation, based on actual weather conditions. These results highlight the importance of selecting durable hydrophilic solar cell cover.

1. Introduction

Solar PV technology provided 592 TWh of electrical energy worldwide in 2018. It is expected to deliver about 4700 TWh by 2040 representing 13% of the projected global energy consumption [1]. Photovoltaic solar cells can be classified as (1) crystalline silicon-based solar cells with efficiency up to 27.6%, (2) thin-film solar cells with efficiency up to 23.4%, (3) emerging solar cells such as dye-sensitized, perovskite, quantum dot, and organic solar cells with an efficiency of up to 25.2%, and (4) multijunction solar cells with efficiency up to 39.2% [2]. Among these different types, crystalline silicon-based solar cells (monocrystalline and polycrystalline) have the highest market share representing more than 90% [3,4].

Outdoor PV solar panels are exposed to the elements including dust, rain, and/or dew that can reduce their efficiency, power output, and lifetime [5–8]. The adverse effect of soiling by dust on solar cell performance has been widely documented [9–13]. Jiang et al. [9] showed experimentally that the conversion efficiency of amorphous silicon PV cells can be reduced by 26% for a dust deposition density of 22 g/m^2 of PV cell under normally incident irradiance of 760 W/m^2 supplied by a solar simulator. Pavan et al. [10] compared the power output of polycrystalline silicon PV cells built on either sandy (more dusty) or compact (less dusty) soils. The power output losses, compared with clean PV cells, were 6.9% and 1.1% for sandy and compact soil sites, respectively. In addition, a few studies considered the effect of rainfall on the dust-covered PV solar cell performance [11–13]. These studies showed that rain helps wash off the dust accumulated on the cells and thus improves their performance compared with the dust-covered PV solar cells [11–13].

Dew formation refers to water vapor condensing on a surface at a temperature below the dew point temperature of the surrounding air or even above due to (i) the presence of hygroscopic dust on the PV module glass cover [14] and/or (ii) capillary effects [15]. It has been shown to occur 15%–95% of the nights in the grasslands of the United States and last for hours under high relative humidity conditions [16]. Dew formation results in droplet accumulation that eventually evaporates during the day upon warming of the air and direct heating by solar

* Corresponding author. Mechanical and Aerospace Engineering Department, University of California, Los Angeles, Los Angeles, CA, 90095-1597, USA.
E-mail address: pilon@seas.ucla.edu (L. Pilon).

https://doi.org/10.1016/j.solmat.2020.110908
Received 11 August 2020; Received in revised form 5 November 2020; Accepted 1 December 2020

Nomenclature

d	droplet diameter (μm)
d_p	projected droplet diameter (μm)
f_A	surface area coverage (%)
G_s	solar irradiation (W/m^2)
H	height (mm)
i	current (mA)
I	intensity (W/m^2 sr)
k	absorption index
L	length (mm)
m	complex index of refraction, $m = n + ik$
n	refractive index
P_h	hourly electrical energy production rate (W/m^2)
$P_{\max}$	maximum power (mW)
R	reflectance (%)
r_c	radius of curvature
S_C	total radiation flux (kW/m^2)
T	temperature (°C)
t	time (hr)
u_w	wind velocity (m/s)
V	voltage (V)
W	width (mm)

Greek Symbols

θ_B	Brewster angle (°)
θ_c	contact angle (°)
θ_{cr}	critical angle (°)
θ_i	incident angle (°)
θ_r	reflection angle (°)
θ_T	tilt angle (°)
θ_t	transmission angle (°)
η	solar cell energy conversion efficiency (%)

Subscription

a	air
ac	air/solar cell interface
ag	air/glass interface
c	solar cell
d	droplet
dew	dew point
g	glass
ga	glass/air interface
gd	glass/droplet interface
gc	glass/solar cell interface
p	p-polarized light
r	ratio
s	s-polarized light

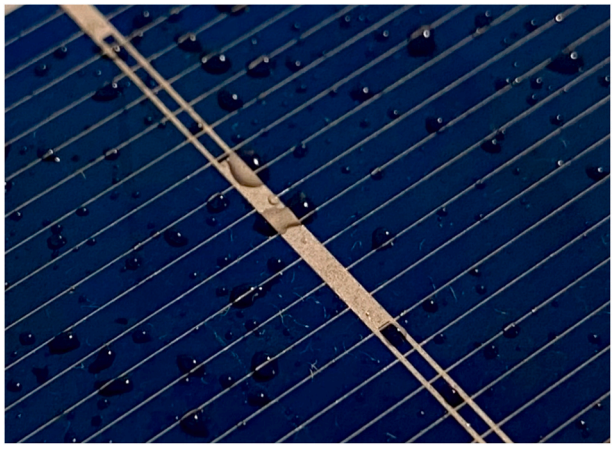

Fig. 1. Photograph of a PV solar cell covered with water droplets from dew or rain.

radiation. Dew formation is also significant in semi-arid coastal regions such as in the province of Almería in southeast Spain where dew forms more than 75% of the nights [17] and where deployment of large photovoltaic systems are envisioned to power the largest concentration of greenhouses in Europe and reduce greenhouse gas emissions [18]. In general, water droplets due to dropwise condensation (as well as rain) can be frequently observed at the surface of PV solar cells, as illustrated in Fig. 1. Dew formed at night can remain during the day until it evaporates while solar cells generate power. For example, Guo et al. [19] reported the presence of dew for up to 7-h during the day in the desert-shrub ecosystem of northwestern China in July. To the best of our knowledge, only a few studies have investigated the effect of dropwise condensation on the performance of PV cells [14,20–22]. Ilse et al. [14] reported frequent dew formation on the surface of outdoor PV modules in arid regions with high concentrations of airborne dust. The presence of dew was found to increase dust and particle adhesion onto the surface of the PV cells and thus reduce their performance and increase maintenance costs. Figgis et al. [21] also demonstrated experimentally that dew formed on soiled PV modules even when the PV module surface temperature was higher than the dew point temperature. This was attributed to the fact that hygroscopic materials such as salt, nitrate, and sulfate found in the dust particles serve as nucleation sites for dropwise condensation of atmospheric water vapor. The power output of the PV solar cells was also shown to decrease under high relative humidity weather conditions due to the scattering of solar radiation by the water vapor in the atmosphere and by condensed droplets formed on the solar cell surface [23].

Hosseini et al. [24] investigated experimentally the effect of dew formation on the performance of monocrystalline and polycrystalline silicon solar cells. LEDs were used to provide radiation between 400 and 1100 nm with total irradiation up to 309 W/m^2 under normal incidence onto horizontal solar cells. Humidifier and heater/cooler units were used to regulate the humidity and temperature of the air in the test chamber. The relative humidity was varied from 45 to 75%. The chamber temperature was imposed above the dew point temperature of 25 °C to study dry solar cells and (ii) below 25 °C to investigate solar cell covered with droplets with surface area coverage ranging between 45 and 84%. The maximum power output of the module was found to increase by 3.5% and 7% in the presence of droplets at a relative humidity of 75% for monocrystalline and polycrystalline cells, respectively. This was attributed to the increase in the number of photons reaching the solar cell since the scattering of the incident radiation by water vapor in the ambient air decreased with dew formation. Finally, the maximum power decreased by about 9% for a polycrystalline solar cell as the droplet surface area coverage increased from 45% to 84% by increasing the relative humidity from 45% to 75%, respectively. Unfortunately, despite the valuable insights, the contact angle and size distribution of the droplets were not reported in this study. Also, the droplet surface area coverage could vary during the experiments due to the evaporation and/or condensation. In addition, the droplet contact angle and/or surface area coverage might have been different for the monocrystalline and polycrystalline solar cells. This could explain why the percentage increase in the maximum power output of the polycrystalline solar cells was greater than the monocrystalline solar cells under the same relative humidity. Finally, all the performance metrics reported corresponded to

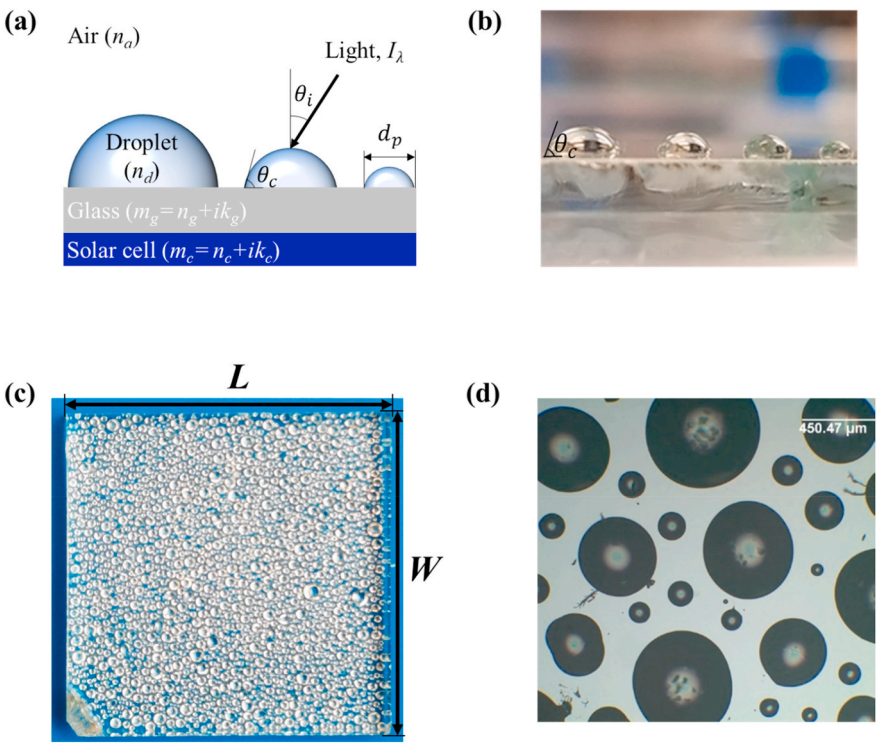

Fig. 2. (a) Schematic of a solar cell with a semi-transparent glass cover supporting transparent polydisperse droplets, (b) side view photograph of acrylic droplets with mean contact angle $\overline{\theta}_c = 76.2°$, (c) photograph, and (d) microscope image of the Teflon AF-2400 coated semi-transparent glass cover with acrylic droplets with droplet mean contact angle $\overline{\theta}_c = 76.2°$ and surface area coverage $f_A = 45\%$.

normal incidence radiation when the effect of droplets on the transmittance of the glass cover has been shown to be relatively limited [25].

Overall, most of the previous studies reported in the literature have not considered systematically the effect of incident angle, droplet contact angle, and/or droplet surface area coverage on the solar cell performance. However, in the absence of a sun tracking system, the angle of incidence of solar radiation on stationary solar cells varies during the course of the days and seasons. In particular, at incident angles larger than 30° with respect to the normal direction of the PV cell surface, the transmittance of droplet-covered glass cover decreases drastically for most droplet contact angles [25]. In addition, the surface of the glass cover may be affected by the environmental conditions (e.g., dirt accumulation, damages, rain, and/or dew). Then, under these different conditions, a wide range of droplet contact angle and surface area coverage may be observed in practice. Therefore, the present study investigates experimentally the effect of droplet surface coverage and contact angle on the performance of solar cells under simulated collimated solar radiation with a wide range of incident angles. To do so, bare polycrystalline silicon solar cells with different glass covers supporting droplets with various contact angles and surface area coverage were tested.

2. Materials and methods

2.1. Materials preparation and characterization

Bare polycrystalline silicon solar cells (Aoshike, China) with a surface area of 3.8 × 3 cm^2 and a maximum power of 175 W/m^2 were used as representative of commercially available solar cells deployed in the field. Three types of solar cell assembly were tested including (1) the bare solar cell as received, (2) the solar cell covered with a clear soda-lime glass cover, and (3) the bare solar cell with a clear soda-lime glass cover without or with surface treatment and covered with acrylic droplets.

Commercial 3 mm thick plane-parallel slabs of soda-lime architectural glass with a surface area of 2.5 × 2.5 cm^2 were used as cover. The glass covers were placed on top of the bare solar cell and the rest of the solar cell was covered with opaque black tape to match the glass size. Three different surface-treatment conditions were investigated to achieve different droplet contact angles including (A) clean soda-lime glass cover, (B) soda-lime glass cover coated with a silane-treated monolayer of silica nanoparticles, and (C) soda-lime glass cover coated with Teflon AF-2400 (Chemours, USA). First, all glass covers were cleaned with isopropyl alcohol (IPA) prior to any surface treatment or droplet deposition. Before coating the glass covers with a monolayer of silane-treated silica nanoparticles, the covers were placed on a hot plate at 450 °C for 30 min to remove any oil, dirt, and organic residues. Silica nanoparticles with 307 ± 20 nm diameter were synthesized by the Stöber process [26,27]. The details of the silica nanoparticle synthesis are given in Supplementary Material. The ethanol/water-based silica nanoparticle suspension was sonicated to break down any nanoparticle aggregate. Then, the suspension was drop-casted onto the glass covers [28] to obtain a monolayer of silica nanoparticles with an arithmetic average surface roughness of 35 nm measured with Atomic Force Microscope (Bruker, Dimension FastScan). The coated glass covers were heat-treated on a hot plate at 450 °C for 1 h to bond the nanoparticles onto the glass surface and make the coating mechanically robust. Finally, silane was deposited on top of the monolayer of silica nanoparticles by placing the glass covers inside a closed container filled with silane vapor. The silane reacted with the available hydroxyl group (OH) and permanently grafted perfluorocarbon chains on the surface of the nanoparticles and glass substrate to form a hydrophobic monolayer [29]. The third type of glass covers were spin-coated with Teflon AF-2400 followed by heat-treatment on a hot plate at 250 °C for an hour. Finally, the sample was baked in a furnace at 340 °C for 3.5 h to achieve a 50 nm thick Teflon film [30].

Following the preparation of the glass covers without or with surface-treatment, thousands of transparent acrylic droplets made of

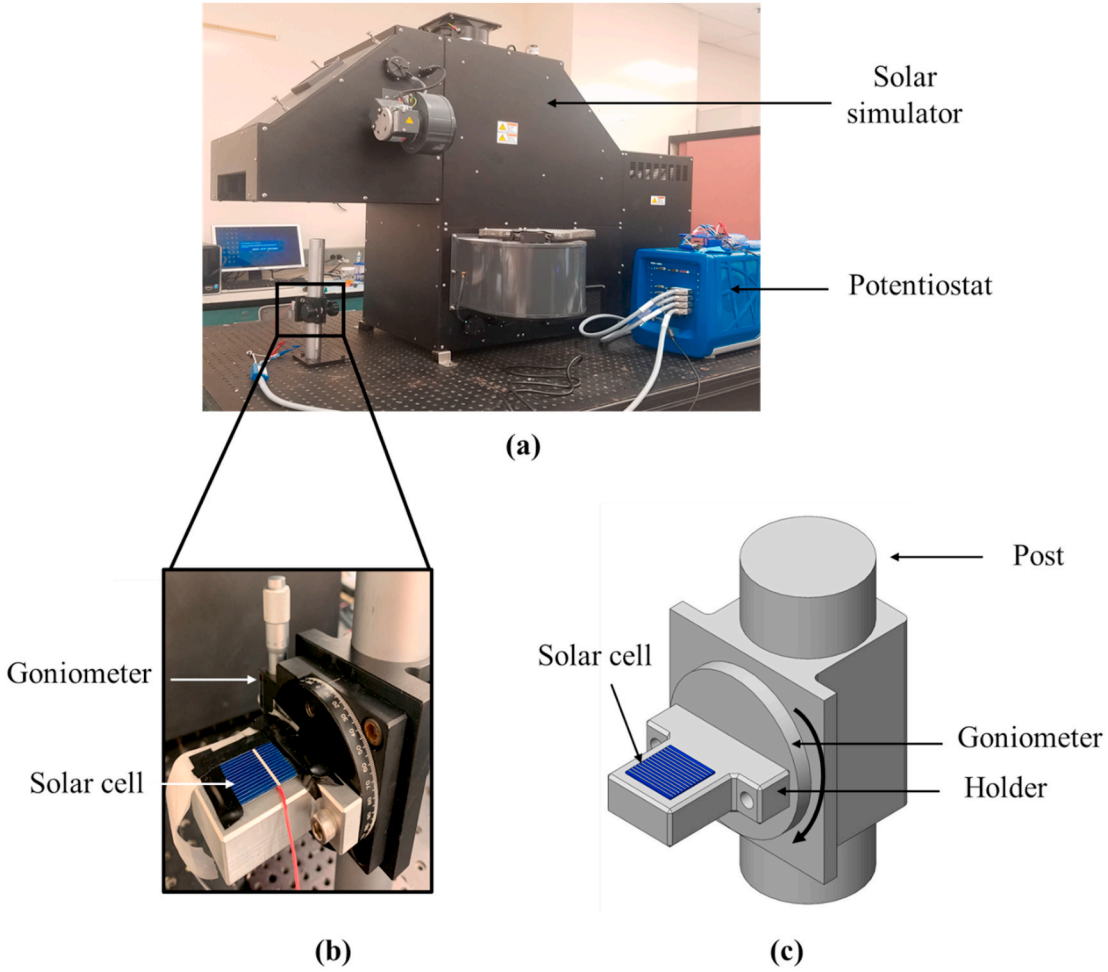

Fig. 3. (a) Photograph of the experimental setup with the solar simulator (TriSol TS-300, OAI, USA) and the sample holder, (b) goniometer supporting a polycrystalline silicon solar cell assembly, and (c) detailed schematic of the goniometer stage. (For interpretation of the references to color in this figure legend, the reader is referred to the Web version of this article.)

ultraviolet (UV) curable acrylic polymer (Loctite AA 349) were deposited onto the glass covers with a syringe and cured with a UV lamp at 365 nm (Blak-Ray B-100 A, Thermo Scientific Fisher, USA). The use of polymer droplets instead of water droplets facilitated the handling of the solar cell assemblies and eliminated the challenges caused by the dynamic nature of dropwise condensation and water evaporation. In addition, when handling the solar cell or when tilting it to simulate non-normal incidence, the water droplets would merge and/or roll-off from the glass surface. Acrylic presented the benefit of being relatively viscous to avoid excessive spreading and merging among droplets during deposition over the glass substrate and was easily UV-curable without any color change. Overall, by using acrylic droplets, the surface area coverage and size distribution could be carefully characterized for each sample and remained the same throughout the experiments.

The contact angle of acrylic droplets on the glass cover was measured using a Drop Shape Analyzer (DSA100, Kruss Scientific, Germany). For each type of glass substrate, the contact angle measurements were repeated for 9 different droplets and the mean contact angle $\overline{\theta}_c$ was calculated. The projected diameter d_p and surface area coverage f_A of the droplets were measured using microscope images captured by a Leica LMIL microscope (Leica Microsystems, USA) connected to a CCD camera (Spot Insight model 4.2, USA). The image analysis software ImageJ was used in manual mode to measure the location and projected diameter of a large number of droplets.

Fig. 2(a) schematically shows a solar cell with a semi-transparent glass cover supporting droplets along with the geometric parameters characterizing the droplets. The acrylic droplets had a refractive index n_d of about 1.49 in the visible [31] falling between that of air ($n_a = 1$) and that of soda-lime glass ($n_g \approx 1.53$) [32]. Thus, the optical effects caused by the presence of the acrylic droplets are expected to be qualitatively similar to that of water droplets despite the difference in their refractive indices (1.49 vs. 1.33). Indeed, our previous study [25] established that the directional-hemispherical transmittance of glass cover supporting droplets with contact angle $\theta_c = 90°$ and surface area coverage $f_A = 50\%$ followed the same trends and was quantitatively similar for droplets with refractive index n_d equal to 1.33 or 1.5, as illustrated in Fig. S1. The polycrystalline silicon solar cells had a refractive index n_c of about 3.90 and absorption index k_c of about 0.03 in the visible [33]. Fig. 2(b) shows a side view of the acrylic droplets with droplet mean contact angle $\overline{\theta}_c = 76.2°$. Finally, Figs. 2(c) and 2(d) present the photograph and microscope image of the Teflon-coated semi-transparent glass cover with acrylic droplets with droplet mean contact angle $\overline{\theta}_c = 76.2°$ and surface area coverage $f_A = 45\%$.

2.2. Solar cell performance characterization

Figs. 3(a) and 3(b) show the experimental setup consisting of (i) a polycrystalline silicon solar cell assembly mounted on (ii) a goniometer (OptoSigma, USA) with a custom made sample holder, (iii) a solar simulator (TriSol TS-300, OAI, USA) providing collimated simulated solar radiation in the wavelength range between 400 and 1100 nm with total radiation flux incident on a surface perpendicular to the collimated

Table 1
Summary of the solar cell assemblies tested in this study.

Sample #	Sample details	Incident angle θ_i (°)	Droplet contact angle $\overline{\theta}_c$ (°)	Droplet surface area coverage f_A (%)	Droplet projected diameter $\overline{d}_p$ (μm)
1	Cell without glass	0–85	N/A	N/A	N/A
2	Cell with dry glass	0–85	N/A	0	N/A
3	Cell with droplet-covered glass	0–85	76.2	45	312
4	Cell with droplet-covered glass	0–85	76.2	34	271
5	Cell with droplet-covered glass	0–85	76.2	19	428
6	Cell with droplet-covered glass	0–85	66.6	47	250
7	Cell with droplet-covered glass	0–85	25.8	49	614

simulated radiation of $S_c = 1$ kW/m^2, and (iv) a potentiostat (BioLogic VSP-300, France) used to collect the current vs. voltage curves (*i-V* curves) of the different solar cell assemblies investigated under different angles of incidence. Fig. 3(c) shows the detailed schematic of the goniometer stage and of the sample holder used to vary the incident angle θ_i of the simulated solar radiation. Before any measurement, each solar cell assembly was securely taped flat onto the sample holder.

Finally, two metrics were considered to assess the performance of any given solar cell assembly namely (a) the maximum power $P_{\max}$ and (ii) the energy conversion efficiency η defined as [34]

$$P_{max} = Max(iV) \text{ and } \eta = \frac{P_{max}}{G_s}. \quad (1)$$

Here, G_s is the solar irradiation incident on the PV cell at incident angle θ_i and expressed as $G_s = S_c\cos\theta_i$. The solar cell temperature remained constant at near room temperature (~22 °C) throughout the experiments. In fact, the *i-V* curve for the bare solar cell was recorded regularly to verify that the solar cell temperature and incident simulated solar irradiation remained constant throughout the experiment, as documented in Fig. S2 in Supplementary Material.

3. Results and discussion

3.1. Droplet characterization

The different glass covers were characterized in our previous study [35]. Table 1 summarizes the mean contact angle $\overline{\theta}_c$ and surface area coverage f_A for the seven different solar cell assemblies tested under simulated solar irradiation G_s with incident angle θ_i varying between 0 (normal incidence) and 85° corresponding to G_s varying between 1 kW/m^2 and 0.087 kW/m^2, respectively. The droplet mean contact angle on (A) clean, (B) silane-treated silica nanoparticle-coated, and (C) Teflon-coated glass covers were $\overline{\theta}_c = 25.8°$, 66.6°, and 76.2°, respectively. The droplet mean projected diameter d_p on different glass covers varied between 250 μm and 614 μm while the surface area coverage f_A ranged between 19% and 49% [35].

3.2. Solar cell performance

3.2.1. i-V curves

Fig. 4 compares the *i-V* curves obtained from (i) a bare solar cell, (ii) a solar cell with dry glass cover, and (iii) a solar cell with glass covers supporting droplets with mean contact angle $\overline{\theta}_c = 25.8°$, 66.6°, and 76.2° for (a) incident angle $\theta_i = 0°$ and irradiation $G_s = 1$ kW/m^2, (b) $\theta_i = 30°$ and $G_s = 0.86$ kW/m^2, (c) $\theta_i = 50°$ and $G_s = 0.64$ kW/m^2, and (d) $\theta_i = 70°$ and $G_s = 0.34$ kW/m^2. Here, the droplet surface area coverage f_A of the glass covers was around $f_A = 47 \pm 2\%$ for all solar cell assemblies considered to isolate the effects of θ_i and $\overline{\theta}_c$ on the solar cell performance.

First, for all incident angles, the bare solar cell systematically featured the largest current *i* for any potential *V*. Thus, it can serve as a reference to assess the effects of the glass cover and droplets on the solar cell performance. Figs. 4(a) and 4(b) indicate that the glass cover reduces the generated current across the potential window of the solar cell by about 15%. This relatively large decrease was due to the iron content of the conventional soda-lime glass used and can be considered as an upper bound. In fact, thinner and/or ultra-clear glass cover would reduce significantly the effect of the dry glass cover. In addition, the presence of droplets did not affect the *i-V* curve of the solar cells under near-normal incident radiation ($\theta_i \leq 30°$). This can be explained by the fact that most of the collimated light incident at angle $\theta_i \leq 30°$ was transmitted through the glass cover supporting droplets, as established numerically by Zhu et al. [25]. These experimental results also corroborate the experimental observations reported in the literature indicating that the droplets did not significantly affect the performance of solar cells under normal incidence [36,37]. By contrast, Figs. 4(c) and 4(d) establish that, for incident angles $\theta_i = 50°$ and 70°, the generated current *i* decreased significantly due to the presence of droplets, particularly as the droplet contact angle $\overline{\theta}_c$ increased from 25.8° to 76.2°. This observation can be attributed to the decrease in the number of photons reaching the photovoltaic solar cell surface due to the increase in reflectance caused by the presence of droplets [34,38]. Additional experiments were performed by spraying water droplets, using a push spray bottle, on the glass cover of the same solar cell used throughout the study (see Supplementary Materials). The results established that the *i-V* curves of the solar cell with glass cover sprayed with water droplets were quantitatively similar to those obtained when the glass cover supported acrylic droplets, as illustrated in Fig. S3. However, the droplet surface area coverage f_A and projected diameter d_p could not be determined as they varied due to rapid droplet evaporation at near-normal incident angles and/or droplet merger and roll-off for larger incident angles.

Fig. 5 schematically illustrates light transfer through the solar cell assembly with (a) dry glass cover and (b) droplet-covered glass cover under normal collimated incident radiation. Photons that reached the air/glass interface with incident angle θ_i were refracted through the air/glass interface with the transmission angle $\theta_{t,1}$ before reaching the glass/solar cell interface. The latter has a reflectivity to unpolarized light expressed as [39]

$$R_{gc} = (R_s + R_p)/2. \quad (2)$$

where R_s and R_p are the reflectivities of the interface for s-polarized and p-polarized light predicted by Fresnel equations considering the glass to be non-absorbing and the solar cell to be absorbing [39]. The reflectivity R_{gc} of the glass/solar cell interface remained nearly constant around 19% for incident angle θ_i ranging from 0 to 85° (see Supplementary Materials). *In absence of droplets*, the photons reflected by the glass/solar cell interface traveled through the glass window and were reflected back towards to solar cell due to internal reflection at the glass/air interface with critical angle $\theta_{cr,ga} = \sin^{-1}(n_a/n_g) \approx 41°$ [39] [Fig. 5(a)]. The multiple reflections through the glass cover increase the probability of the photons to eventually be absorbed by the solar cells. By contrast, *in presence of droplets*, the reflected photons were transmitted into the droplets through the glass/droplet interface because of the small index

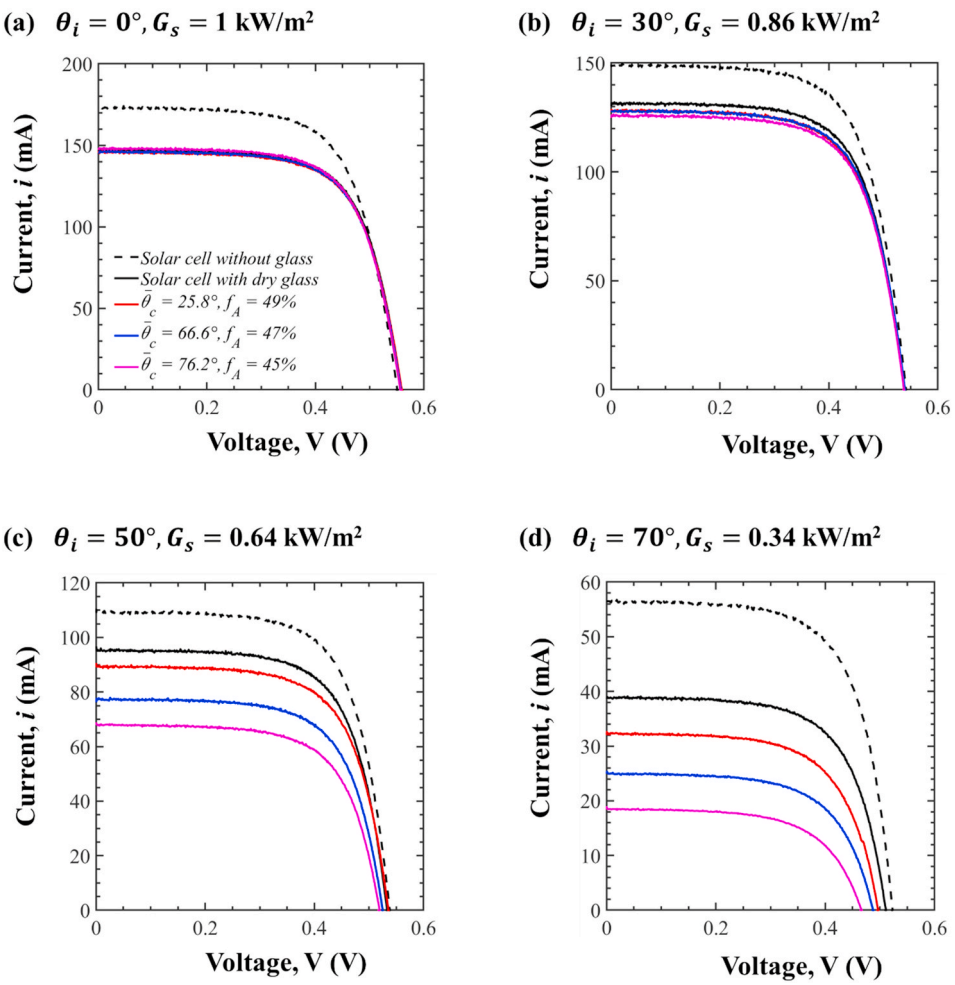

Fig. 4. Current as a function of voltage for (a) incident angle $\theta_i = 0°$ and irradiation $G_s = 1$ kW/m^2, (b) $\theta_i = 30°$and $G_s = 0.86$ kW/m^2, (c) $\theta_i = 50°$and $G_s = 0.64$ kW/m^2, and (d) $\theta_i = 70°$ and $G_s = 0.34$ kW/m^2.

mismatch between the glass and the droplets corresponding to a large critical angle $\theta_{cr,gd} = \sin^{-1}(n_d/n_g) \approx 77°$ [39] [Fig. 5(b)]. Then, due to the droplet curvature, the photon reached the droplet/air interface at an angle smaller than the critical angle of that interface $\theta_{cr,da} = \sin^{-1}(n_a/n_d) \approx 39°$ and were transmitted through the interface. Note that reflection losses were very similar at the air/glass and air/droplet interface so the number of photons entering the solar cell assembly was not significantly affected by the presence of droplets. In addition, reflection loss at the droplet/glass interface was negligible due to the very small index mismatch. Overall, the presence of droplets resulted in back-scattering of incident photons instead of trapping and photovoltaic conversion.

Furthermore, Figs. 4(c) and 4(d) indicate that, for surface coverage $f_A \approx 47\%$ and large incident angle $\theta_i \geq 50°$, the generated current decreased with increasing droplet mean contact angle $\bar{\theta}_c$. Figs. 5(c) and 5 (d) schematically illustrate the effect of the droplet contact angle on the number of photons reaching the solar cell surface. The number of photons transmitted through the droplet/air interface increased with increasing droplet contact angle due to the fact that the photon incident angle on the droplet/air interface decreased with decreasing droplet radius of curvature defined as $r_c = d/2 \sin\bar{\theta}_c$. As a result, less photons were reflected back towards the solar cell and the generated cell current decreased. Note that, only for droplet contact angles $\bar{\theta}_c \geq 76.2°$, the photons that were incident at large angles could experience total internal reflection at the droplet/air interface and then reached the solar cell. Zhu et al. [25] numerically showed that, for water droplets condensed at the frontside of windows, total internal reflection at the droplet/air interface occurred for droplet contact angles $\theta_c \geq 70°$ and large incident angles, i.e. for $\theta_c = 70°$ total internal reflection occurred for incident angles $\theta_i > 80°$.

3.2.2. Maximum power

Fig. 6(a) shows the maximum power P_{max} generated by the solar cell as a function of the incident angle θ_i for the three different assemblies considered. Here also, the droplet mean contact angles considered were $\bar{\theta}_c = 25.8°$, 66.6°, or 76.2° while the surface area coverage f_A was maintained around 47 ± 2%. Fig. 6(a) indicates that, for a solar cell, bare or with a dry glass cover, the maximum power P_{max} decreased with increasing incident angle θ_i [40]. In fact, the maximum power generated by the solar cell closely follows the same trend as the incident solar irradiation $G_s = S_c \cos\theta_i$ and has been expressed as [41]

$$P_{max}(\theta_i) = P_{max}(\theta_i = 0)\cos\theta_i \cdot \quad (3)$$

Fig. 6(a) establishes that the measured maximum power of bare solar cell P_{max} was in excellent agreement with the predictions of Equation (3). However, the measured maximum power of solar cells with a dry glass cover slightly deviated from Equation (3) for incident angles $\theta_i \geq 50°$. This can be attributed to the increase in the reflection losses for incident angle θ_i larger than the Brewster angle θ_B. Indeed, the reflectivity of the air/glass interface to incident unpolarized light remained nearly constant for $\theta_i < \theta_B$ and then increased sharply for $\theta_i > \theta_B$ where the Brewster angle is equal to $\theta_{B,ag} = tan^{-1}(n_g/n_a) \approx 57°$ [39]. On the other hand, the Brewster angle for the bare solar cell was $\theta_{B,ac} =$

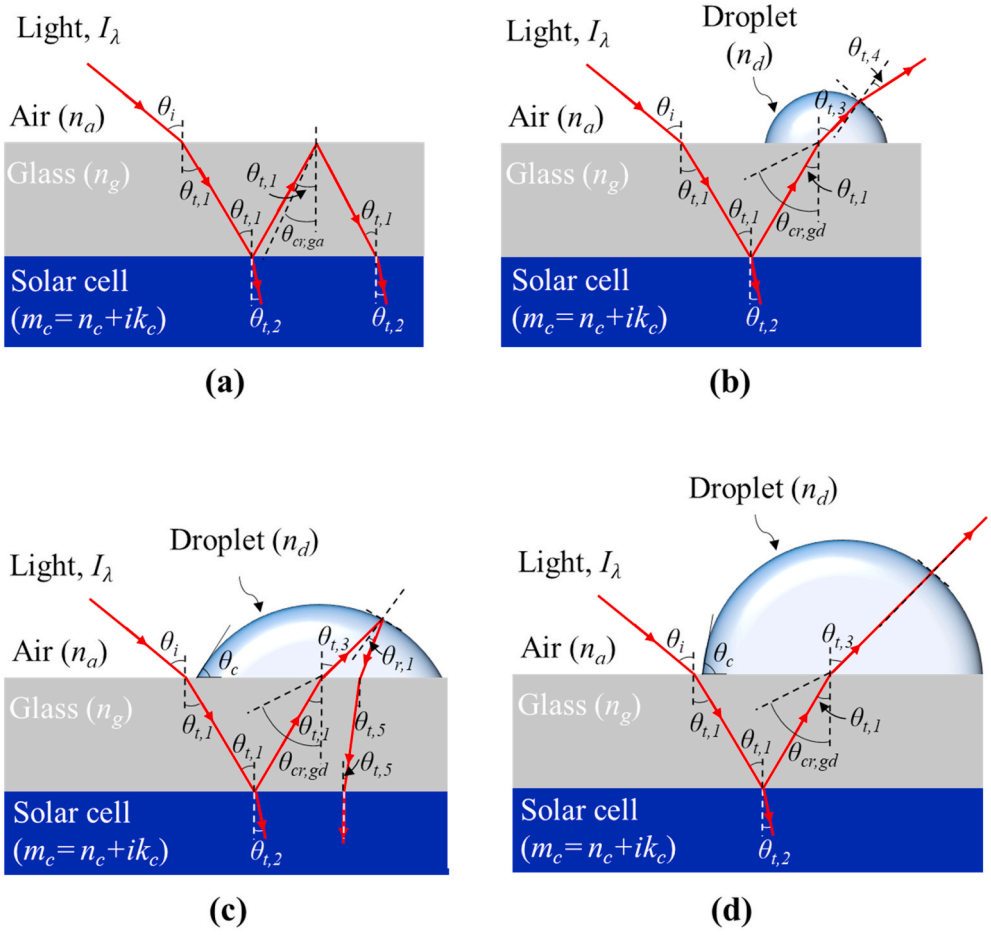

Fig. 5. Schematic of a solar cell with (a) dry glass cover and (b) droplet-covered glass cover to explain the effect of droplets on the light transmittance and a solar cell with droplet-covered glass cover having (c) small droplet contact angle and (d) large droplet contact angle to demonstrate the effect of droplet contact angle on the light transmittance under collimated incident radiation at angle θ_i.

$tan^{-1}(n_c/n_a) \approx 74^\circ$. In addition, the maximum power P_{max} of the solar cells was unchanged for dry and droplet-covered glass covers under normal incidence ($\theta_i = 0^\circ$). These results corroborate the observations of Hosseini et al. [24] for monocrystalline solar cells. Fig. 6(a) also establishes that, in the presence of droplets, the maximum power P_{max} decreased with increasing droplet contact angle $\overline{\theta}_c$ for incident angles $\theta_i > 30^\circ$ because of the optical phenomena invoked previously (Fig. 5).

3.2.3. Solar cell energy conversion efficiency

Fig. 6(b) shows the solar cell energy conversion efficiency η [Equation (1)] as a function of the incident angle θ_i for the same three configurations considered previously with similar surface area coverage f_A around 47% but different droplet contact angles $\overline{\theta}_c$ between 25.8° and 76.2°. Fig. 6(b) indicates that for $0^\circ \leq \theta_i \leq 30^\circ$, the energy conversion efficiency η remained constant and identical for all solar cell assemblies with a glass cover with or without droplets. However, for $\theta_i > 30^\circ$, the energy conversion efficiency η decreased with increasing incident angle θ_i and droplet contact angle $\overline{\theta}_c$. For example, for $\theta_i = 60^\circ$, the energy conversion efficiency decreased from $\eta = 10\%$ for a dry glass cover to 9% and 5% for droplet mean contact angle $\overline{\theta}_c$ of 25.8° and 76.2°, respectively. This decrease in the energy conversion efficiency can be attributed to the decrease in the maximum power output of the PV solar cell, as previously discussed [Fig. 6(a)].

Moreover, it is interesting to note that, for $\overline{\theta}_c = 76.2^\circ$ and $f_A = 45\%$, the solar cell energy conversion efficiency η decreased with increasing incident angle θ_i until it reached a minimum at $\theta_i = 80^\circ$ beyond which it increased. This was due to the fact that transmittance of the solar irradiance through the glass cover supporting droplets increased at large incident angles ($\theta_i > 80^\circ$), thus improving the energy conversion efficiency. In fact, this behavior was also observed by Zhu et al. [25] in the numerically predicted directional hemispherical transmittance through a 3 mm thick glass slab supporting water droplets with contact angle $\theta_c \geq 70^\circ$. The authors attributed this behavior to the decrease in total internal reflection at the back window/air interface and to the increase in internal reflection at the droplet/air interfaces for glazing incident angles θ_i [25].

To isolate the effect of droplet surface area coverage f_A on the solar cell efficiency η, we define the efficiency ratio $\eta_r(\theta_i, \overline{\theta}_c, f_A)$ as the ratio of the energy conversion efficiency of the solar cell with droplet-covered glass $\eta(\theta_i, \overline{\theta}_c, f_A)$ to that of the dry glass cover $\eta(\theta_i, f_A = 0)$ under the same incident angle θ_i, i.e.,

$$\eta_r\left(\theta_i, \overline{\theta}_c, f_A\right) = \eta\left(\theta_i, \overline{\theta}_c, f_A\right) \Big/ \eta(\theta_i, f_A = 0). \quad (4)$$

Fig. 7 plots the energy conversion efficiency ratio $\eta_r(\theta_i, \overline{\theta}_c, f_A)$ as a function of incident angle θ_i for a solar cell with a droplet-covered glass cover with mean contact angle $\overline{\theta}_c = 76.2^\circ$ and $f_A = 19$, 34, and 45%. Fig. 7 indicates that the efficiency ratio η_r decreased significantly due to the presence of droplets for incident angle $\theta_i > 30^\circ$. The decrease was more significant for larger surface area coverage f_A. In fact, the presence of droplets caused the solar cell efficiency to decrease by up to 50–70% compared to a dry glass cover, for the range of f_A considered. This was due to the fact that an increasingly large fraction of the incident light was back-scattered as the droplet surface coverage f_A increased, as

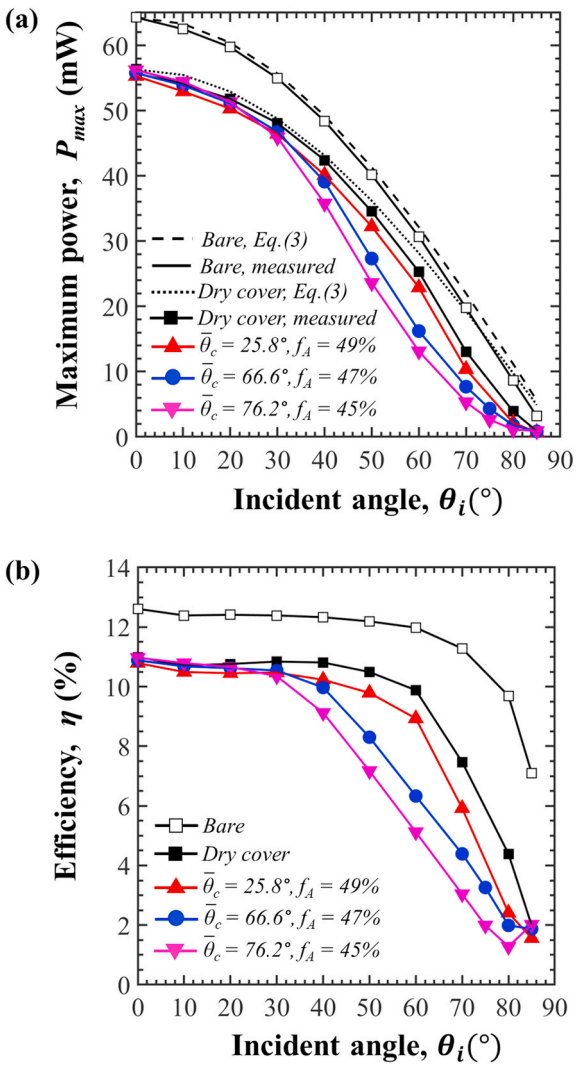

Fig. 6. (a) Maximum power P_{max} and (b) energy conversion efficiency η as functions of incident angle θ_i for the solar cell without glass cover, with dry glass cover, and with droplet-covered glass cover droplet mean contact angle $\overline{\theta}_c$ = 25.8°, 66.6°, and 76.2° and surface area coverages f_A = 45, 47, and 49%, respectively.

previously explained. Note that for $\theta_i > 80°$, the solar cell with a droplet-covered glass cover with f_A = 45% featured a slightly higher efficiency than the solar cell with a dry glass cover as droplets scattered the light back towards the solar cell.

3.3. Impact of dew formation on hourly energy generation

Dew formation occurs at night [16,17] and is frequently observed on PV modules in the morning hours [42–44]. For certain locations/seasons, dew formation can persist during daytime depending on weather conditions such as high humidity and wind speed [19,45], and field conditions such as the presence of hygroscopic dust [21]. To assess the impact of droplets on the power generation of solar cells deployed in the field, let us consider a field of PV solar cells located in San Francisco, CA (latitude: 37°N; longitude: 122°W) in December. San Francisco was selected for the widespread deployment of residential solar PV power generation in California [46] and the frequent dew formation [47]. In order to predict the energy generated per unit surface area of PV solar cells, the following assumptions were made: (i) PV solar cells were facing South with the optimum tilt angle of $\theta_T = 30°$ [48,49]. (ii) the PV solar cell temperature T_c (in °C) was predicted according to [50]

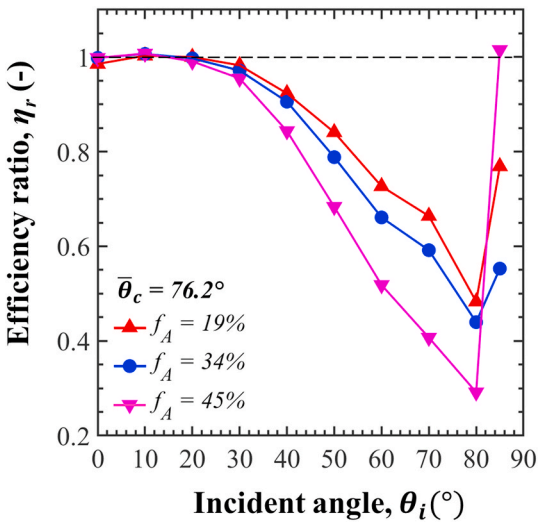

Fig. 7. Energy conversion efficiency ratio η_r as a function of incident angle θ_i for solar cell with droplet-covered glass cover having a droplet contact angle $\overline{\theta}_c$ = 76.2° and surface area coverages f_A = 19, 34, 45%.

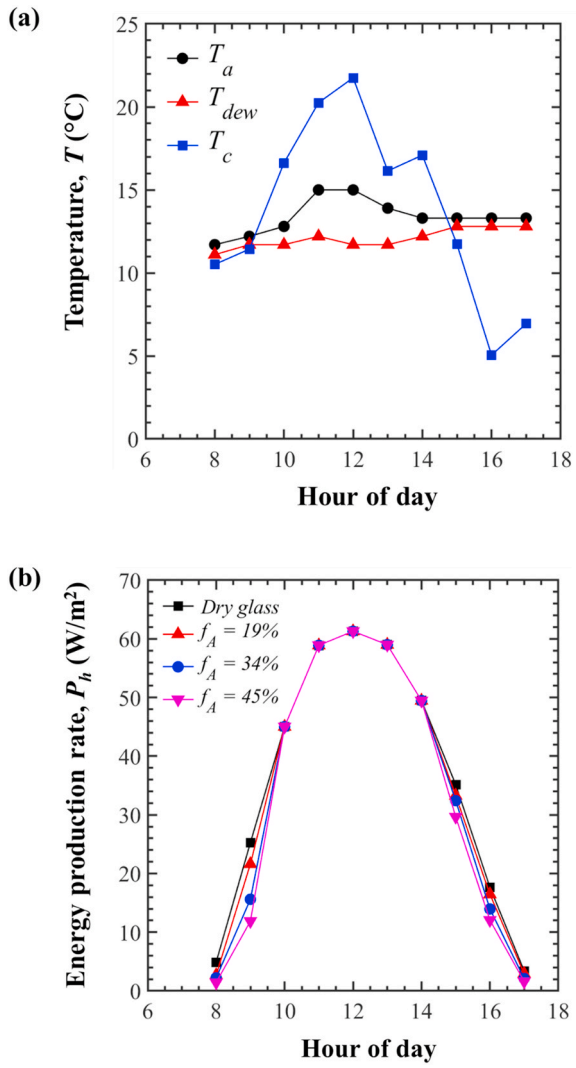

Fig. 8. Hourly (a) ambient, dew point, and solar cell temperatures and (b) energy production rate on December 3 as functions of the hour in San Francisco, CA.

$$T_c(t) = 0.943T_a(t) + 0.028G_s(t) - 1.528u_w(t) + 4.3\cdot \quad (5)$$

Here, T_a is the ambient air temperature (in °C) and u_w is the wind velocity (in m/s). The average hourly solar irradiation and incident angle for a 30° tilted PV solar cell in San Francisco were taken from Ref. [51] and Ref. [52], respectively. The hourly weather hygrometric and wind speed data for San Francisco averaged over several years were taken from Ref. [53].

Moreover, the average hourly electrical energy production rate P_h (in W/m^2) can be expressed as

$$P_h(\theta_i(t)) = G_s(\theta_i)\eta\left(\theta_i, \overline{\theta}_c, f_A\right)\cdot \quad (6)$$

where the incident angle $\theta_i(t)$ depends on the time of the day and $\eta(\theta_i, \overline{\theta}_c, f_A)$ is the energy conversion efficiency previously measured for the different solar cell assembly configurations.

Fig. 8 shows the hourly (a) ambient air $T_a(t)$, dew point, and PV cell $T_c(t)$ temperatures (in °C) and (b) average hourly electrical energy production rate (W/m^2) predicted by Equation (6) for a solar cell with (i) dry glass cover and (ii) droplet-covered glass cover with droplet mean contact angle $\overline{\theta}_c = 76.2°$ and surface area coverage $f_A = 19$, 34, and 45% on December 3. The use of hydrophobic coatings has been recommended for PV module glass covers [54–58] as a practical way to reduce dust adhesion [56–59] and remove soiling during droplet roll-off [60–62]. In addition, hydrophobic coatings inhibit condensation [21] and can be designed to reduce light reflection [60]. Therefore, the droplet contact angle $\overline{\theta}_c = 76.2°$ was taken as a baseline for our calculations. Figs. 8(a) and 8(b) indicate that the dew formation resulted in a drop in the average hourly electrical energy production rate in the morning and afternoon. For example, the energy generation at 9:00 a.m. decreased by 14%, 38%, and 53% for droplet mean contact angle $\overline{\theta}_c = 76.2°$ and surface area coverage $f_A = 19$, 34, and 45% compared with the solar cells with dry glass covers, respectively. Note that cleaning of the dust accumulated on hydrophobic PV modules thanks to dew roll-off and/or rain was not considered. In addition, the temporal changes in the droplet surface area coverage due to the evaporation and/or condensation and tilting the PV module was not considered. Finally, differences in the droplet surface area coverage for hydrophilic and hydrophobic glass covers was not accounted for.

Overall, these results suggest that dew or rain can significantly affect the performance of solar cell particularly in the morning or afternoon when the solar radiation is incident at angle $\theta_i > 30°$. Hydrophilic covers or coatings can limit the negative effect of droplets provided their hydrophilicity can be maintained throughout the lifetime of the solar cells.

4. Conclusion

This study investigated experimentally the effect of droplets on the performance of PV solar cells due to dropwise condensation or rain falling on their glass cover. Polydisperse acrylic droplets were deposited on glass covers subjected to different surface treatments. The droplet contact angle was varied between 25° and 77° and their surface area coverage between 19% and 49%. The photovoltaic solar cells with a dry or droplet-covered glass cover were exposed to collimated simulated solar radiation with radiation flux up to 1 kW/m^2 with incident angle θ_i ranging between 0 and 85°. For incident angle $\theta_i \leq 30°$, the droplets had no effect on the generated current, the maximum power, and the energy conversion efficiency of the solar cells. However, for incident angle $\theta_i > 30°$, the droplet significantly decreased the solar cell performance, particularly for large droplet contact angle and/or the surface area coverage. This was attributed to the fact that the incident light was back-scattered through the droplets instead of being trapped due to total internal reflection at the cover/air interface before being eventually absorbed by the solar cell. In addition, the study showed that the hourly energy production may decrease significantly with dew formation on the solar cell cover, based on actual weather conditions. These results highlight the importance of selecting durable hydrophilic solar cell cover.

CRediT authorship contribution statement

Eylul Simsek: Conceptualization, Investigation, Visualization, Writing - original draft, Writing - review & editing. **Megan J. Williams:** Investigation, Data curation, Writing - original draft. **Laurent Pilon:** Supervision, Conceptualization, Writing - review & editing.

Declaration of competing interest

The authors declare that they have no known competing financial interests or personal relationships that could have appeared to influence the work reported in this paper.

Acknowledgment

ES is grateful to The Scientific and Technological Research Council of Turkey (TÜBİTAK). The authors would like to thank (i) Prof. P. Kavehpour and S. Andalib for their assistance in measuring the droplet contact angles, (ii) Prof. S. H. Tolbert and N. Kashanchi for the synthesis of silica nanoparticles, (iii) Dr. M. Marszewski for his help with the silane coating, (iv) Asahi Glass Corporation for supplying the glass substrates, (v) L. Tokunaga from California NanoSystems Institute at UCLA, and (vi) D. Turan for their help with the Teflon coating and AFM images.

Appendix A. Supplementary data

Supplementary data to this article can be found online at https://doi.org/10.1016/j.solmat.2020.110908.

References

[1] International Energy Agency (IEA), World Energy Outlook, Last accessed on May 5, 2020 via: https://www.iea.org/reports/world-energy-outlook-2019.
[2] National Renewable Energy Laboratory, Best Research-Cell Efficiency Chart, Last accessed on May 5, 2020 via: https://www.nrel.gov/pv/cell-efficiency.html.
[3] M. Fischer, Trends & Challenges in c-Si PV - an update of the ITRPV 9th ed., in World Solar Congress, Shanghai, China, September 4–5, 2018, pp.1–22.
[4] A. Abdulkadir, A.A. Aziz, M.Z. Pakhuruddin, Impact of micro-texturization on hybrid micro/nano-textured surface for enhanced broadband light absorption in crystalline silicon for application in photovoltaics, Mater. Sci. Semicond. Process. 105 (2020) 104728.
[5] F.M. Zaihidee, S. Mekhilef, M. Seyedmahmoudian, B. Horan, Dust as an unalterable deteriorative factor affecting PV panel's efficiency: why and how, Renew. Sustain. Energy Rev. 65 (2016) 1267–1278.
[6] H.A. Kazem, M.T. Chaichan, Effect of environmental variables on photovoltaic performance-based on experimental studies, International Journal of Civil, Mechanical and Energy Science 2 (5) (2016) 1–8.
[7] M. Santhakumari, N. Sagar, A review of the environmental factors degrading the performance of silicon wafer-based photovoltaic modules: failure detection methods and essential mitigation techniques, Renew. Sustain. Energy Rev. 110 (2019) 83–100.
[8] N.S.M. Hussin, N.A.M. Amin, M.J.A. Safar, R.S. Zulkafli, M.S.A. Majid, M.A. Rojan, I. Zaman, Performance factors of the photovoltaic system: a review, MATEC Web of Conferences 225 (2018) 1–8.
[9] H. Jiang, L. Lu, K. Sun, Experimental investigation of the impact of airborne dust deposition on the performance of solar photovoltaic (PV) modules, Atmos. Environ. 45 (25) (2011) 4299–4304.
[10] A.M. Pavan, A. Mellit, D. De Pieri, The effect of soiling on energy production for large-scale photovoltaic plants, Sol. Energy 85 (5) (2011) 1128–1136.
[11] H.K. Elminir, A.E. Ghitas, R.H. Hamid, F. El-Hussainy, M.M. Beheary, K.M. Abdel-Moneim, Effect of dust on the transparent cover of solar collectors, Energy Convers. Manag. 47 (2006) 3192–3203.
[12] R. Appels, B. Lefevre, B. Herteleer, H. Goverde, A. Beerten, R. Paesen, K.D. Medts, J. Driesen, J. Poortmans, Effect of soiling on photovoltaic modules, Sol. Energy 96 (2013) 283–291.
[13] M.R. Maghami, H. Hizam, C. Gomes, M.A. Radzi, M.I. Rezadad, S. Hajighorbani, Power loss due to soiling on solar panel: a review, Renew. Sustain. Energy Rev. 59 (2016) 1307–1316.
[14] K.K. Ilse, B.W. Figgis, V. Naumann, C. Hagendorf, J. Bagdahn, Fundamentals of soiling processes on photovoltaic modules, Renew. Sustain. Energy Rev. 98 (2018) 239–254.

[15] G. Yang, D. Chai, Z. Fan, X. Li, Capillary condensation of single- and multicomponent fluids in nanopores, Ind. Eng. Chem. Res. 58 (41) (2019) 19302–19315.
[16] F. Ritter, M. Berkelhammer, D. Beysens, Dew frequency across the US from a network of in situ radiometers, Hydrol. Earth Syst. Sci. 23 (2) (2019) 1179–1197.
[17] O. Uclés, L. Villagarcía, M.J. Moro, Y. Canton, F. Domingo, Role of dewfall in the water balance of a semiarid coastal steppe ecosystem, Hydrol. Process. 28 (4) (2014) 2271–2280.
[18] A. Carreño-Ortega, E. Galdeano-Gómez, J.C. Pérez-Mesa, M.D.C. Galera-Quiles, Policy and environmental implications of photovoltaic systems in farming in southeast Spain: can greenhouses reduce the greenhouse effect? Energies 10 (6) (2017).
[19] X. Guo, T. Zha, X. Jia, B. Wu, W. Feng, J. Xie, J. Gong, Y. Zhang, H. Peltola, Dynamics of dew in a cold desert-shrub ecosystem and its abiotic controls, Atmosphere 7 (3) (2016) 1–15.
[20] K.K. Ilse, B.W. Figgis, M. Werner, V. Naumann, C. Hagendorf, H. Pollmann, J. Bagdahn, Comprehensive analysis of soiling and cementation processes on PV modules in Qatar, Sol. Energy Mater. Sol. Cell. 186 (2018) 309–323.
[21] B. Figgis, A. Nouviaire, Y. Wubulikasimu, W. Javed, B. Guo, A. Ait-Mokhtar, R. Belarbi, S. Ahzi, Y. Remond, A. Ennaoui, Investigation of factors affecting condensation on soiled PV modules, Sol. Energy 159 (2018) 488–500.
[22] K. Ilse, B. Figgis, M.Z. Khan, V. Naumann, C. Hagendorf, Dew as a detrimental influencing factor for soiling of PV modules, IEEE Journal of Photovoltaics 9 (1) (2019) 287–294.
[23] H.A. Kazem, M.T. Chaichan, Effect of humidity on photovoltaic performance based on experimental study, Int. J. Appl. Eng. Res. 10 (23) (2015) 43572–43577.
[24] S.A. Hosseini, A.M. Kermani, A. Arabhosseini, Experimental study of the dew formation effect on the performance of photovoltaic modules, Renew. Energy 130 (2019) 352–359.
[25] K. Zhu, S. Li, L. Pilon, Light transfer through windows with external condensation, J. Quant. Spectrosc. Radiat. Transf. 208 (2018) 164–171.
[26] W. Stöber, A. Fink, E. Bohn, Controlled growth of monodisperse silica spheres in the micron size range, J. Colloid Interface Sci. (1968) 62–69.
[27] K. Nozawa, H. Gailhanou, L. Raison, P. Panizza, H. Ushiki, E. Sellier, J.P. Delville, M.H. Delville, Smart control of monodisperse Stöber silica particles: effect of reactant addition rate on growth process, Langmuir 21 (4) (2005) 1516–1523.
[28] M. Mannini, Molecular Magnetic Materials on Solid Surfaces, Firenze University Press, Firenze, Italy, 2008.
[29] S. Ebnesajjad, C. Ebnesajjad, Surface Treatment of Materials for Adhesive Bonding, second ed., Elsevier Science, 2014.
[30] J. Scheirs (Ed.), Modern Fluoropolymers High Performance Polymers for Diverse Applications, John Wiley & Sons, New Jersey, NJ, 1997.
[31] G. Beadie, M. Brindza, R.A. Flynn, A. Rosenberg, J.S. Shirk, Refractive index measurements of poly(methyl methacrylate) (PMMA) from 0.4 – 1.6 μm, Appl. Optic. 54 (31) (2015) 139–143.
[32] M. Rubin, Optical properties of soda lime silica glasses, Sol. Energy Mater. 12 (4) (1985) 275–288.
[33] M.A. Green, Self-consistent optical parameters of intrinsic silicon at 300 K including temperature coefficients, Sol. Energy Mater. Sol. Cell. 92 (2008) 1305–1310.
[34] S.A. Kalogirou, Solar Energy Engineering: Processes and Systems, Academic Press, London, UK, 2009.
[35] E. Simsek, K. Zhu, N. Kashanchi, M.J. Williams, T. Galy, M. Marszewski, S. H. Tolbert, L. Pilon, Light transfer through semi-transparent glass panes supporting pendant droplets, manuscript submitted for publication, 2020.
[36] D. Dahlioui, B. Laarabi, M.A. Sebbar, A. Barhdadi, Soiling effect on photovoltaic modules performance: new experimental results, in: International renewable and sustainable energy conference (IRSEC), Marrakech, Morocco, November 14-17, 2016.
[37] S.A. Sulaiman, A.K. Singh, M.M.M. Mokhtar, M.A. Bou-Rabee, Influence of dirt accumulation on performance of PV panels, Energy Procedia 50 (2014) 50–56.
[38] H. Baig, H. Kanda, A.M. Asiri, M.K. Nazeeruddin, T. Mallick, Increasing efficiency of perovskite solar cells using low concentrating photovoltaic systems, Sustainable Energy and Fuels 4 (2) (2020) 528–537.
[39] J.R. Howell, R. Siegel, M.P. Mengüc, Thermal Radiation Heat Transfer, 5th ed., CRC Press, New York, NY, 2010.
[40] P. Mialhe, S. Mouhamed, A. Haydar, The solar cell output power dependence on the angle of incident radiation, Renew. Energy 1 (3–4) (1991) 519–521.
[41] H.L. Willis, W.G. Scott, Distributed Power Generation: Planning and Evaluation, Marcel Dekker, New York, NY, 2000.
[42] W. Luo, Y.S. Sheng, P. Hacke, V. Naumann, D. Lausch, S.V. Harvey, J.P. Singh, J. Chai, Y. Wang, A.G. Aberle, S. Ramakrishna, Potential-induced degradation in photovoltaic modules: a critical review, Energy Environ. Sci. 10 (1) (2017) 43–68.
[43] R.R. Corder, A. Damiani, D. Laroze, S. MacDonell, J. Jorquera, E. Sepúlveda, S. Feron, P. Llanillo, F. Labbe, J. Carrasco, J. Ferrer, G. Torres, Effects of soiling on photovoltaic (PV) modules in the Atacama Desert, Sci. Rep. 8 (1) (2018) 1–14.
[44] A. Sayyah, M.N. Horenstein, M.K. Mazumder, Energy yield loss caused by dust deposition on photovoltaic panels, Sol. Energy 107 (2014) 576–604.
[45] B. Khalil, J. Adamowski, A. Shabbir, C. Jang, M. Rojas, K. Reilly, B. Ozga-Zielinski, A review: dew water collection from radiative passive collectors to recent developments of active collectors, Sustainable Water Resources Management 2 (1) (2016) 71–86.
[46] Cape Analytics, Cape Analytics Data Report: The Most Solar Places in America, Last accessed on October 28, 2020 via: https://capeanalytics.com/cape-analytics-data-report-the-most-solar-places-in-america/.
[47] Current Results Weather and Science Facts, Most humid cities in the United States. https://www.currentresults.com/Weather-Extremes/US/most-humid-cities.php. (Accessed 28 October 2020).
[48] C.S. Sanchez J, C.L. Cheng, Verification of optimal angle for south orientated tilted plans according to the latitude, concept for BIPV. Proceedings of ISES Solar World Congress, in: D.Y. Goswami, Y. Zhao (Eds.) 2, 2007. Beijing, China, September 18–21, 2007.
[49] C.L. Cheng, C.S. Sanchez Jimenez, M.C. Lee, Research of BIPV optimal tilted angle, use of latitude concept for south orientated plans, Renew. Energy 34 (6) (2009) 1644–1650.
[50] R. Chenni, M. Makhlouf, T. Kerbache, A. Bouzid, A detailed modeling method for photovoltaic cells, Energy 32 (9) (2007) 1724–1730.
[51] European Comission, Photovoltaic Geographical Information System (PVGIS), Last accessed on June 01, 2020 via: https://ec.europa.eu/jrc/en/pvgis.
[52] National Renewable Energy Laboratory, Solar position and intensity (SOLPOS), Last accessed on June 05, 2020 via: https://midcdmz.nrel.gov/solpos/solpos.html.
[53] Energy Design Tools, Climate Consultant, Energy Design Tools, Last accessed on June 26, 2020 via: http://www.energy-design-tools.aud.ucla.edu/.
[54] G.C. Oehler, F. Lisco, F. Bukhari, S. Ulicna, B. Strauss, K.L. Barth, J.M. Walls, Testing the durability of anti-soiling coatings for solar cover glass by outdoor exposure in Denmark, Energies 13 (2) (2020) 1–17.
[55] M. Fathi, M. Abderrezek, M. Friedrich, Reducing dust effects on photovoltaic panels by hydrophobic coating, Clean Technol. Environ. Policy 19 (2) (2017) 577–585.
[56] Y.Y. Quan, L.Z. Zhang, Experimental investigation of the anti-dust effect of transparent hydrophobic coatings applied for solar cell covering glass, Sol. Energy Mater. Sol. Cell. 160 (2017) 382–389.
[57] Y. Yuan, Y. Chen, W.L. Chen, R.J. Hong, Preparation, durability and thermostability of hydrophobic antireflective coatings for solar glass covers, Sol. Energy 118 (2015) 222–231.
[58] M.A.M.L. de Jesus, G. Timò, C. Agustín-Sáenz, I. Braceras, M. Cornelli, A. de M. Ferreira, Anti-soiling coatings for solar cell cover glass: climate and surface properties influence, Sol. Energy Mater. Sol. Cell. 185 (2018) 517–523.
[59] K. Isbilir, F. Lisco, G. Womack, A. Abbas, J.M. Walls, Testing of an anti-soiling coating for PV module cover glass, IEEE 7th World Conference on Photovoltaic Energy Conversion, 2018, pp. 3426–3431. Hawaii, June 10-15.
[60] S. Sutha, S. Suresh, B. Raj, K.R. Ravi, Transparent alumina based superhydrophobic self–cleaning coatings for solar cell cover glass applications, Sol. Energy Mater. Sol. Cell. 165 (2017) 128–137.
[61] S. Maharjan, K. Liao, A.J. Wang, K. Barton, A. Haldar, N.J. Alley, H.J. Byrne, S. A. Curran, Self-cleaning hydrophobic nanocoating on glass: a scalable manufacturing process, Mater. Chem. Phys. 239 (2020), 122000.
[62] A. Pan, H. Lu, L.Z. Zhang, Experimental investigation of dust deposition reduction on solar cell covering glass by different self-cleaning coatings, Energy 181 (2019) 645–653.